

AD-A076 100

NEW YORK UNIV N Y DEPT OF PHYSICS

F/G 7/4

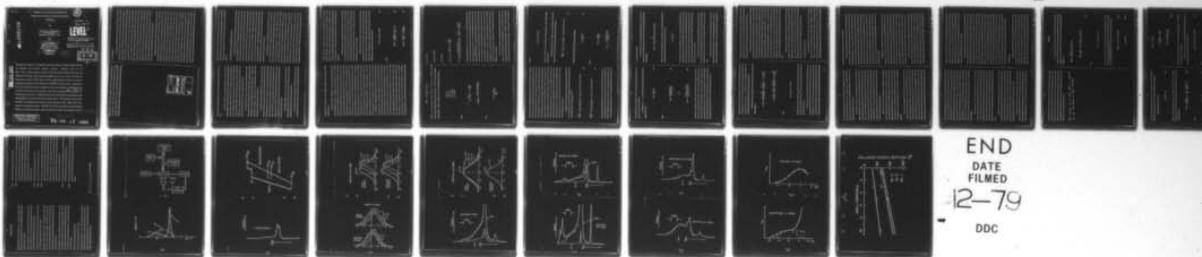
THE EFFECTS OF VELOCITY-CHANGING COLLISIONS ON TWO-PHOTON AND S--ETC(U

SEP 79 P R BERMAN , P F LIAO , J E BJORKHOLM N00014-77-C-0553

UNCLASSIFIED

NL

|OF|
AD
A076100



END
DATE
FILMED
12-79
DDC

6 The Effects of Velocity-Changing Collisions on Two-photon and Stepwise Absorption Spectroscopic

Lineshapes

by

P. F. Liao J. E. Bjorkholm
Bell Laboratories
Holmdel, New Jersey 07733

and

10 F. R. Berman
Physics Department
New York University
New York, N. Y. 10003

11 Sept 1979

ABSTRACT

12

Submitted to
Phys. Rev. A

LEVEL II

Supported by the U.S. Office of Naval Research
under Contract No. N00014-77-C-0553

15
Reproduction in whole or in part is permitted
for any purpose of the United States Government.

DDC
RECEIVED
NOV 2 1979
B

We report the results of an experimental study of the effects of velocity-changing collisions on two-photon and stepwise absorption lineshapes. Excitation spectra for the $3S_{1/2} \rightarrow 3P_{1/2} \rightarrow 4D_{3/2}$ transitions of sodium atoms undergoing collisions with foreign gas perturbers are obtained. These spectra are obtained with two cw dye lasers. One laser, the pump laser, is tuned 1.6 GHz below the $3S_{1/2} \rightarrow 3P_{1/2}$ transition frequency and excites a nonthermal longitudinal velocity distribution of excited $3P_{1/2}$ atoms in vapor. Absorption of the second (probe) laser is used to monitor the steady state excited state distribution which is a result of collisions with rare gas atoms. The spectra are obtained with various He, Ne, and Kr gases and are fit to a theoretical model which utilizes either the phenomenological Keilson-Storer or the classical hard sphere collision kernel. The theoretical model includes the effects of collisionally aided excitation of the $3P_{1/2}$ state as well as effects due to fine-structure state-changing collisions. Although both kernels are found to predict lineshapes which are in reasonable agreement with the experimental results, the hard sphere kernel is

DDC FILE COPY

DISTRIBUTION STATEMENT A

Approved for public release;
Distribution Unlimited

406 850
79 09 17 080

found superior as it gives a better description of the effects of large angle scattering for heavy perturbers. Neither kernel provides a fully adequate description over the entire lineprofile. The experimental data is used to extract effective hard-sphere collision cross sections for collisions between sodium $3P_{1/2}$ atoms and helium, neon and krypton perturbers.

I. INTRODUCTION

Using tunable narrowband lasers, one can selectively excite a narrow nonthermal longitudinal velocity distribution in an atomic or molecular vapor. Collisions between these atoms or molecules and other atoms in the gas cause this distribution to thermalize. A study of the manner in which the collisions modify the distribution leads to an increased understanding of the collisions. In this paper we report the results of a systematic study of the effects of collisions on lineshapes obtained in sodium using two-photon spectroscopy with a resonant intermediate state. These measurements, which are made with two cw dye lasers, yield values for the equivalent hard sphere elastic scattering cross sections for collisions between sodium atoms in the $3P_{1/2}$ state and rare gas perturbers. Comparisons of the experimental lineshapes are made with a theory which utilizes either a classical hard sphere collision kernel or the Keilson-Störmer collision kernel. The theory accounts for the presence of fine-structure state-changing collisions as well as velocity-changing collisions. The validity of these collision models is discussed in light of the experimental data.

Measurements of the effects of velocity-changing collisions on laser spectroscopic lineshapes have been made for some time.^{1,2} In a typical experiment, one monitors the steady-state velocity distribution of atomic levels subjected to nonthermal excitation by a narrowband laser. The degree of velocity thermalization achieved in these states as a result of collisions is determined by the number of collisions occurring within the lifetime of the states and the strength of the collisions. Most previous experiments have been analyzed under the assumptions that the collisions are either of a "weak" or "strong" nature. In the case of "weak" collisions, the collisions which occur during an atom's lifetime have only a small effect on the atomic velocity,³ whereas, in the "strong" collision limit, those atoms which have experienced collisions are assumed to have a thermal distribution. Recently the problem of collisions intermediate to the two limits has received increased attention.² In this case, atoms which experience collisions reach a thermal velocity distribution only if they have several collisions within their lifetime. Because of the short lifetime of the excited atoms in our experiment (16 nsec.), the excited sodium atoms never reach a thermal distri-

ACCESSION for	
NTIS	White Section <input checked="" type="checkbox"/>
DDC	Buff Section <input type="checkbox"/>
UNANNOUNCED	<input type="checkbox"/>
JUSTIFICATION	
BY	PER LETTER
DISTRIBUTION/AVAILABILITY CODES	
Dist.	AVAIL. and/or SPECIAL
A	

spectroscopic lineshapes. In Section III we compare two kernels (Keilson-Sjöfer⁶ and classical hard sphere) that can be used to describe velocity-changing collisions. Our experimental results and a comparison with theory using these collision kernels are then discussed in Section IV.

II. BASIC PRINCIPLES AND EXPERIMENTAL SETUP

The effect of collisions on the lineshapes associated with three-level systems has been treated recently⁷ and the following discussion will be based largely on those results. Our experimental situation is, in fact, somewhat more complicated than the simple three-level case due to the presence of additional levels. While these additional levels are not coupled by the laser radiation fields to the other states, collisions can cause transitions between these levels and the states of interest. Furthermore, the theory given in Reference 7 is valid only in the limits of low intensities. Our actual experiment utilized intensities which often exceed the saturation intensity of a transition and require a more accurate theory to completely describe it. A detailed discussion of this more complete theory is given elsewhere.⁸ In what follows, we give only an outline of the basic principles of the experiment and present the major theoretical results.

Our experimental data are obtained using the experimental setup shown in Figure 1. We use two cw single-mode dye lasers; one (the pump) is set at a fixed angular frequency, Ω , which is tuned to the wing of the Doppler-broadened $3S_{1/2} - 3P_{1/2}$ transition, and the other (the probe), of frequency Ω' , is scanned to complete transitions to the $4D_{3/2}$ state. Transitions to $4D_{5/2}$ are weak in comparison with those to $4D_{3/2}$, because of dipole selection rules which forbid $3P_{1/2} \rightarrow 4D_{5/2}$ transitions, and are neglected. The unfocused beams from the two lasers propagate in opposite directions through a cell at 200°C containing sodium vapor. Typical laser intensities are 0.5 W/cm^2 , and each beam is linearly polarized in the same direction. The sodium vapor density is held between $10^{10} - 10^{11} \text{ cm}^{-3}$ so that resonant reabsorption of atomic fluorescence was not significant and sodium-sodium collisions could be neglected. We monitor the population of the $4D_{3/2}$ state by measuring the intensity of fluorescence at $\sim 330 \text{ nm}$ which occurs when the $4D_{3/2}$ state decays via the

transition so that the measured steady-state velocity distribution shows a "persistence of velocity".

The manner in which the atoms change velocities as a result of collisions is directly dependent on the strength and form of the interaction between the active atom and the perturber atom. Hence, measurements of the thermalization process yield information about the interaction potentials. At the present time we have analyzed our experimental results to obtain the equivalent hard sphere cross sections for sodium in collision with helium, neon, or krypton rare gas atoms. This choice of perturbers allows us to observe the effect of different active atom to perturber atom mass ratios.

Our measurements are made by selectively exciting a particular velocity distribution of sodium atoms to the $3P_{1/2}$ excited state. This excitation is accomplished by tuning a cw dye laser to the wing of the Doppler-broadened $3S_{1/2} - 3P_{1/2}$ transition. A second laser is then scanned to produce $3P_{1/2} - 4D_{3/2}$ transitions. The resulting lineshape directly reflects the longitudinal velocity distribution of the $3P_{1/2}$ state.

In the absence of velocity-changing collisions, one might expect only those atoms which have longitudinal velocities such that they are Doppler-shifted into resonance with the laser frequency would be excited. However, the presence of phase-interrupting collisions results in an excitation of all the velocity groups. In this nonresonant excitation, the energy defect or excess between the atomic transition energy and the laser photon energy is provided or removed by a collision.^{4,5} This nonresonant collisionally-assisted excitation results in population of velocity groups other than those desired and must be accounted for properly in the final analysis of the lineshape.

State-changing collisions such as those which produce transitions between the $3P_{1/2}$ and $3P_{3/2}$ fine-structure states are also found to play an important role. Our analysis is therefore made to account for the effects of such collisions.

In the following section we briefly discuss our experimental setup and the underlying principles involved in obtaining a description of the collision-induced modification of

of atoms which have the correct velocity so as to be Doppler shifted into resonance decreases exponentially. Hence at detunings much greater than the Doppler width, component c will dominate, while at small detunings component b will dominate. We have recently made a detailed study of the collisional redistribution by phase-changing collisions for the case where Ω is tuned far from the resonance so that the other component b is negligible.⁵

The level scheme which is appropriate for our experiments is shown in Figure 3. We generally follow the notation of References 7 and 8 so that state 1 is the $3S_{1/2}$ ground state, state 3 is the $4D_{3/2}$ final state and state 2 is the $3P_{1/2}$ intermediate state. We also allow for state-changing collisions between the $3P_{1/2}$ and $3P_{3/2}$ (state 4) fine structure states. The laser field at Ω' is assumed to couple only the 2 \rightarrow 3 transition, while that at Ω is assumed to act on only the 1 \rightarrow 2 transition.

A complete theory for the excitation lineshape is given in Reference 8 assuming the probe field to be weak. We shall attempt to fit our data using this theory and hard sphere collision models. For such models, collisions produce relatively large velocity changes for the active atoms (i.e., velocity changes Δu such that $\Omega(\Delta u/c) \gtrsim$ all homogeneous widths). In this limit the line shape is given by⁸

$$I(\Omega) = I_{TP}(\Omega) + I_{SW}(\Omega) \quad (1)$$

where

$$I_{TP}(\Omega) = \frac{2(\chi\chi')^2}{\gamma_A \chi \chi' k^2 v^3} \text{Im} \sum_{j=1}^4 A_j Z(\nu_j) \quad (2)$$

$$I_{SW}(\Omega) = \frac{2(\chi\chi')^2}{\gamma_A \chi \chi' k^2} \text{Im} \int \frac{n_2(\nu x)}{(\nu - \nu_2)} dx \quad (3)$$

4P state back to the ground state. Our results give the $3S_{1/2} \rightarrow 3P_{1/2} \rightarrow 4D_{3/2}$ two-photon excitation spectrum.

The lineshape can be roughly viewed as composed of three parts which are illustrated schematically in Figure 2. Although the three components are not completely independent, one can roughly describe them as arising in the following manner. The narrow component marked a would be present even in the absence of collisions and is composed of two-quantum and stepwise transitions of those atoms which have not undergone velocity-changing collisions in the $3P_{1/2}$ intermediate state. We shall refer to this component as the "two-photon" line. The characteristics of this line have been experimentally⁹ and theoretically¹⁰ studied in great detail. The line is essentially Doppler-free owing to the velocity selectivity of the excitation and the use of oppositely-propagating beams. The component labeled b arises from those atoms which, once excited into the $3P_{1/2}$ state, experience velocity-changing collisions. The collisions modify the initial narrow velocity distribution which was excited by the laser at frequency Ω and cause the distribution to broaden and shift toward equilibrium; this thermalization is mirrored in component b of the probe absorption. In our experiments Ω is not set at the atomic resonance frequency and hence the initial longitudinal velocity distribution is not centered at $v_z = 0$ but at a fairly high $v_z = 10^5$ cm/sec. The final component labeled c, is due to collisionally-aided excitation of the $3P_{1/2}$ excited state. This excitation is essentially non-velocity-selective and therefore is completely Doppler-broadened; the probe absorption from this state has nearly the shape of the equilibrium Voigt profile. It differs from the velocity-changing collision component, b, as it would be present even in the absence of velocity-changing collisions, e.g., if the perturber atoms were much less massive than the sodium atoms. It may be viewed as arising from phase-changing collisions which effectively broaden the atomic resonance of each atom. The exact shape of the excitation spectrum depends on the relative amplitudes of the three components. The components b and c each increase relative to a as the perturber pressure is increased. The ratio of b to c amplitudes depends on Ω . Component b decreases rapidly when Ω is adjusted away from the atomic resonance because the number

$$Z(u) = -\pi^{-1/2} \int_{-\infty}^{\infty} e^{-x^2} |u-x|^{-1} dx$$

$Z(u)$ is the plasma dispersion function $Z(u)$ for $\text{Im } u > 0$ and is $-Z(u)$ for $\text{Im } u < 0$

where $\omega(\nu)$ is the Rabi frequency of the transition $1 \rightarrow 2$ (2-3), u is the most probable

maximum velocity, $k = \frac{\Omega}{c}$, $k' = \frac{\Omega'}{c}$ and $k'' = k'k$. The other quantities are defined as

$$\begin{aligned} r_1 &= a + c, \\ r_2 &= b - c, \\ r_3 &= \Gamma_2/k, \\ r_4 &= -\Gamma_2/k', \\ r_5 &= \Gamma_2/k'k. \end{aligned}$$

where

$$a = \frac{\Gamma_2 \Gamma_3}{k'k}, \quad b = \frac{\Gamma_2 \Gamma_3}{k'k'}$$

$$c = \frac{1}{2} \left[b - a - \sqrt{(b-a)^2 + 4\Gamma_2^2/k'k'} \right].$$

and

$$A_1 = \frac{\Gamma_2 \Gamma_3}{\prod_{j=1}^5 (\Gamma_j - r_j)}$$

$$\gamma_{12} = \bar{\gamma}_{12} + \Gamma_2$$

$$\gamma_{13} = \bar{\gamma}_{13} + \Gamma_3 + \Gamma_2$$

$$\gamma_{23} = \bar{\gamma}_{23} + \Gamma_3$$

$$\gamma_{23} = \bar{\gamma}_{23} + \Gamma_3; \quad \left[\bar{\gamma}_{23} \right]^2 = \bar{\gamma}_{12}^2 + \frac{2\bar{\gamma}_{12}\Gamma_2^2}{\Gamma_3}$$

$$\Gamma_3^{-1} = \frac{\gamma_2 + \Gamma_3(\nu) + 0.5\gamma'}{\Gamma_2 + \Gamma_3(\nu) + 1.5\gamma'} + \frac{1}{\Gamma_1(\nu)} \left[1 - \frac{\gamma_2'}{\gamma_2 + \Gamma_3(\nu)} \right]$$

The detunings are defined as $\Delta = \Omega - \omega$, $\Delta' = \Omega' - \omega'$, where the angular frequencies ω and ω' are the transition frequencies of the ground-to-intermediate and intermediate-to-final states respectively. The decay rates $\bar{\gamma}_{ij}$ are the phenomenological decay constants of the density matrix ρ_{ij} and include the effects of phase-changing collisions. The rate γ_2 is the total natural decay rate out of the intermediate state, γ_2' is the natural decay rate from level 2 to 1, $\Gamma_1(\nu)$ is the rate of velocity-changing collisions for atoms in level 1 and γ' is the $3P_{3/2}$ to $3P_{1/2}$ fine-structure state-changing collision rate. Note that the theory allows for power broadening of the $1 \rightarrow 2$ transition. The population distribution $n_2(\nu)$ of the intermediate state appearing in Equation (3) is determined by the atom-pump field interaction and the effects of velocity-changing collisions. Equation (3) is an approximation valid for the case $k \ll k'$ as in our experiment.

The effect of fine-structure state-changing collisions introduces additional complexities. First, it modifies the power broadening of the $1 \leftrightarrow 2$ transition; second, it may modify the velocity-changing process; and finally, it decreases the effective excitation of state 2 since atoms are transferred from the $3P_{3/2}$ to the $3P_{1/2}$ state. To minimize the

complexities we make the simplifying assumption that the velocity-changing cross section is the same for the two fine-structure states, and that no velocity change occurs in the fine-structure state-changing processes. We have verified that the latter assumption is nearly correct by tuning Ω to the wing of the $3S_{1/2} \rightarrow 3P_{3/2}$ transition and thereby exciting a particular velocity class of atoms into the $3P_{3/2}$ state. Collisions cause some of these atoms to transfer to the $3P_{1/2}$ state. The velocity distribution of the atoms in the $3P_{1/2}$ state is then recorded by scanning Ω' across the region of the $3P_{1/2} \rightarrow 4D_{3/2}$ transition. The resulting excitation spectrum is shown in Figure 4. As can be seen in Figure 4, the spectrum and hence the velocity distribution is concentrated in a small region which corresponds to the initial velocity of the atoms. The small splitting in the line is due to the hyperfine structure of the $3P_{1/2}$ state. The fine structure state change appears to happen with little or no change in velocity, justifying our assumption.

To calculate the signal amplitude we must determine $n_2(v)$, the velocity distribution of the $3P_{1/2}$ state. The equations describing this distribution and the longitudinal velocity distribution, $n_4(v)$, of the $3P_{3/2}$ state are (11)

$$\frac{dn_2(v)}{dt} = -[\gamma_2 + \Gamma_2(v) + \gamma_2]n_2(v) + \gamma_2 n_4(v) + \int W(v, v')n_2(v')dv' + T(v); \quad (4)$$

$$\frac{dn_4(v)}{dt} = -[\gamma_4 + \Gamma_4(v) + \gamma_4]n_4(v) + \gamma_4 n_2(v) + \int W(v, v')n_4(v')dv' \quad (5)$$

where $T(v)$ is the velocity distribution of atoms excited to the $3P_{1/2}$ state by the pump laser. The collision kernel, $W(v, v')$ is defined such that the $W(v, v') dv dt$ is the probability that a collision will cause an atom in level 2 moving with a longitudinal velocity between v and $v + dv$ to change to be between v' and $v' + dv$ during a time interval dt . The rate $\Gamma_2(v)$ is

given by

$$\Gamma_2(v) = \int W(v, v')dv'$$

and $\gamma_2 = \gamma'$ and $\gamma_4 = 0.5 \gamma'$ are the $3P_{1/2} \rightarrow 3P_{3/2}$ and $3P_{3/2} \rightarrow 3P_{1/2}$ collisional transfer rates, respectively.

The equation which gives $n(v) = n_2(v) + n_4(v)$, the longitudinal velocity distribution function for the sum of the population densities of the two $3P$ states is

$$\frac{dn(v)}{dt} = -[\gamma + \Gamma] \int W(v, v')dv' n(v) + \int W(v, v')n(v')dv' + T(v). \quad (6)$$

Equation (6) is easily solved to yield the steady-state solution

$$n(v) = \sum_{v'} \frac{T(v')}{\gamma + \Gamma(v')} \quad (7)$$

where

$$n(v) = \frac{T(v)}{\gamma + \Gamma(v)}$$

$$n^{(v)}(v) = \frac{\int W(v, v')n^{(v')}(v')dv'}{\gamma + \Gamma(v)}$$

The quantity $n^i(v)$ is the population density of atoms having experienced exactly i collisions since initially excited into the $3P$ states.

By substituting $n_1 = n - n_2$ into Equation (4) and using equation (7), we solve equations (4) to obtain

$$n_2(v) = \sum_{j=0}^{\infty} n_j^i(v). \tag{8}$$

where

$$n_j^i(v) = \frac{0.5\gamma^i n(v) + T(v)}{\gamma + \Gamma_j(v) + 1.5\gamma^i}. \tag{9}$$

and

$$n_j^i(v) = \frac{\int W(v',v) n_j^{i-1}(v') dv'}{\gamma + \Gamma_j(v) + 1.5\gamma^i}. \tag{10}$$

In this paper we consider two collision kernels for insertion into equation 10, the Keilson-Störmer and the classical hard sphere kernels. Due to the simple mathematical form of the Keilson-Störmer kernel an analytic expression for $n_2(v)$ can be obtained. However, for the hard sphere kernel it is necessary to calculate $n_2(v)$ numerically. These collision kernels will be discussed in the following section. The distribution $n_2(v)$, given by equations 8-10, is inserted into equation (3) and the total lineshape is then given by equations 1-3.

III. COLLISION KERNELS

All the properties of the velocity-changing collision process are contained in the collision kernel. The most commonly used kernel is the phenomenological kernel of Keilson and Störmer,⁶

$$W(v,v') = \Gamma \left[\pi(\Delta v) \right]^{1/2} \exp \left[-(\nu' - \alpha \nu)^2 / (\Delta v)^2 \right],$$

where Γ is the (speed independent) rate of collisions, α is a parameter which depends on relative masses of the active and perturber atom mass ratio, and

$$\Delta v = \left[1 - \alpha^2 \right]^{1/2} v$$

is $\sqrt{2}$ times the rms velocity change per collision. Borenstein and Lamb¹² compared the Keilson-Störmer kernel with Monte Carlo calculations of hard sphere collisions and found fairly close agreement between the two. However, they were concerned mainly with the cases of light perturbers and small initial velocities (velocities small compared with Doppler width). Recently, more detailed comparisons have been made^{13,14} although again for cases of light perturbers and low velocities.

In this section we shall compare some of the properties of the Keilson-Störmer kernel with the exact analytic expression for the kernel which describes classical collisions between atoms having a hard sphere interatomic potential ($V=0$ for $r>r_0$ and $V=\infty$ for $r<r_0$).

The Keilson-Störmer kernel has the form of a displaced Gaussian whose width and shift are determined by the parameter, α . The method for the determination of α which we utilize is that suggested by LeGouët¹³, in which α is chosen such that the Keilson-Störmer

model gives the same rms velocity change per collision as the analytic hard sphere kernel. This method gives $\alpha = 0.8, 0.4,$ and 0.0 for collisions between sodium and helium, neon and krypton atoms, respectively. A major feature of the Keilson-Störmer kernel is its mathematical simplicity which allows analytic expressions to be obtained.

The hard sphere kernel is considerably more complicated. It is given by the following expression:

$$W(v',v) = \frac{\pi r_0^2}{4} \left(\frac{1+\beta^2}{\beta^2} \right) \left(1 - \text{erf} \left[\left(\frac{1+\beta^2}{2\beta} \right) |S| + \beta \frac{v'}{u} \frac{S}{|S|} \right] \right) + \frac{1}{2} \left[-S \left(S + \frac{2v'}{u} \right) \right] \left(1 - \text{erf} \left[\left(\frac{1-\beta^2}{2\beta} \right) |S| - \beta \frac{v'}{u} \frac{S}{|S|} \right] \right)$$

where

$$\beta^2 = m_p/m_a; \quad S = (v-v')/u.$$

The mass of the active atom (Na) is m_a , and the mass of the perturber atom is m_p . This kernel has been obtained by Kol'chenko,¹⁵ however for completeness we have included its derivation in the Appendix.

To compare the kernels, we plot in Figures 5 to 7 $n^i(v)$ (Equation 7) for sodium calculated with both kernels for helium, neon, and krypton perturbers assuming $\Gamma(v)$ is a delta function at $v/u = 1.6$. In the case of a very light perturber such as helium (Figure 5), the two kernels are quite similar. Each gives distributions $n^i(v)$ which shift more toward equilibrium with each collision, and both models produce distributions with approximately

the same shifts and widths. To allow for easy comparison of the distributions we have normalized the peak of each to unity. In fact, at the pressure (2.5 Torr) used for the calculation, each successive $n^i(v)$ decreases in amplitude by about a factor of 6 or more.

The calculated distributions for the most massive perturber, krypton, show some significant differences. Krypton is 3.7 times heavier than sodium. As in the case of helium, the distributions predicted by the two kernels are quite similar for $i \geq 2$ although the widths of the distributions now predicted by the hard sphere models are significantly larger than those given by the Keilson-Störmer model owing to the speed dependence of $\Gamma(v)$ in the hard sphere model. The greatest difference appears in the distribution $i = 1$. Krypton collisions produce a relatively flat-topped distribution. The amplitude at $v = 0$ is nearly the same as at the initial velocity (taken to be $v_0 = 1.6u$). The Keilson-Störmer distribution, on the other hand, is a factor of 12 larger at $v = 0$ than at v_0 . Note that the velocity distributions produced by the heavier perturber initially broaden and then narrow in the hard sphere model, whereas for the Keilson-Störmer kernel, complete thermalization occurs after one collision.

Comparisons of the distributions calculated using these two kernels indicate the following. First, for heavier perturbers it is at low pressures that the differences are most significant since it is at low perturber pressure that the contribution of $n^1(v)$ to $n(v)$ dominates. Secondly for high perturber pressures the two kernels give nearly the same lineshapes. Our experiments have therefore concentrated on fairly low perturber pressures. In the case of helium we expect the two models to give nearly identical results.

IV. EXPERIMENTAL RESULTS

Excitation spectra were taken of the $3S_{1/2} - 3P_{1/2} - 4D_{3/2}$ transition of atomic sodium vapor for various pressures of helium, neon and krypton buffer gases. In each case, the laser at Ω was adjusted to be 1.6 GHz below the $3S_{1/2} (F=1) - 3P_{1/2}$ transition. Examples of the spectra obtained by sweeping Ω' are given in Figures 8 to 12. In each case, the two narrow lineshape features are the result of the combination of two-quantum and step-

wise transitions originating from the two hyperfine levels of the ground state. The broader feature is the collision-induced signal and, as discussed earlier, is composed of velocity-changed atoms and atoms excited via phase-interrupting collisions. This feature is not present when the perturber gas is removed.

The excitation was made with counter-propagating beams. This geometry was utilized to minimize the linewidth of the two narrow two-photon and stepwise resonances. It is essential that these resonances be narrow so that the collision-induced signals are unobscured. If we use copropagating beams the narrow resonances are split by 390 MHz because of the hyperfine structure of the $3P_{1/2}$ state.⁹ With the use of oppositely-propagating beams, this splitting collapses⁹ to 7 MHz. Some of the spectra contain evidence of resonances due to copropagating beams. These are symmetrically located about $\Delta' = 0$ from the counter-propagating resonances and apparently are the result of stray reflections into the sodium cell. We were unable to completely eliminate them.

We choose to set $\Omega/2\pi$ to be 1.6 GHz below the $3S_{1/2}(F=1) \rightarrow 3P_{1/2}$ transition. With this rather large detuning, the difference between the Keilson-Störmer and hard-sphere kernel which we discussed in Section III¹⁵ are emphasized. Furthermore, the spurious copropagating resonances mentioned above are less troublesome since they occur at the edge of the lineshape of interest. At this detuning the collisional redistribution and velocity changing contributions to the lineshape (components b and c of Figure 2) are comparable in amplitude.

The data were fit to equations (1-3), (8-10) using experimental values of γ_{ij} and γ' obtained from the literature,¹⁶ and a value $\chi/ku = 0.018$ determined from measurements of pump intensity. The lineshape was assumed to arise as an independent sum of contributions originating from both hyperfine ground states. The relative amplitudes of the two narrow resonances were found to be pressure and intensity dependent. This dependence is due to optical pumping effects which modify the population of the ground state hyperfine levels. To account for the optical pumping, the initial relative population of the two states was taken as a free parameter which was adjusted so that the theory correctly

predicted the relative amplitudes of the two narrow resonances.

The only remaining parameter to be determined is the velocity-changing collision cross-section. We obtain values for these cross-sections at each perturber pressure by fitting the ratio of the signal at $\Delta' = 0$ to that at $\Delta/2\pi = 1.6$ GHz. Having fit these two ratios, the overall comparison between the theoretical and experimental profiles can be used to test various collision models. One should note that, for our procedure, the nature of the fit is relatively insensitive to the saturation parameter. This result was verified experimentally by varying the pump power. In our analysis we set the branching ratio $\gamma_2/\gamma_1 = 1$ for both $3P_{1/2} \rightarrow 3S_{1/2}(F=1)$ and $3P_{1/2} \rightarrow 3S_{1/2}(F=2)$ transitions and $\Gamma_1(v)$ to gas kinetic values. The net effect of such an arbitrary choice is to modify the saturation parameter, but, as noted above, this modification has little effect on our fitting procedure. Finally, the assumption of a weak probe field is reasonably well satisfied; signal strength was found to vary linearly with probe power.

Representative data obtained with helium and neon buffer gases are shown in Figures 8 and 9. The results of the theory using both the Keilson-Störmer kernel (open circles) and the classical hard sphere kernel (solid points) are given. As expected, for these lighter perturbers both kernels do nearly equally well in producing fairly-accurate lineshapes. However, for the data with krypton perturbers (Figures 10 to 12) the hard-sphere model does better in predicting the lineshape at the lowest pressure. The theoretical lineshape using the hard-sphere kernel is slightly wider and gives more intensity in the region $\Delta/2\pi = 1$ GHz than does the Keilson-Störmer kernel and hence is in better agreement with the experimental data. Both models fail in the region very close to the narrow resonances.

To obtain curves which are more closely related to the velocity-changing collision kernel, we have attempted to extract from the experimental spectra only that component arising from velocity changing collisions (component b of Figure 2). To extract this component we subtract from the experimental data the theoretical contributions from all other sources. The results of this subtraction are shown in Figures 13 and 14 as Δ_{vc} . The smooth curve represents the experimental points after this subtraction. The solid points give the

theoretical velocity-changing contribution using the hard sphere kernel and the open circles give the same for the Keilson-Störmer kernel. In Figure 13 we show results for the case of helium perturbers at 9.5 Torr. As expected from our earlier discussion, both collision kernels give similar distributions and these are in good agreement with the experimental data. The data for krypton at 1 Torr is given in Figure 14. In this case, the hard-sphere model is clearly superior to the Keilson-Störmer approximation, which produces a lineshape which is too sharply peaked at $\Delta' = 0$. Although the hard-sphere calculation is in excellent agreement in the wing, it also fails for frequencies very near to the narrow resonance. Due to the low pressure the theoretical lineshapes in Figure 14 are dominated by the $i = 1$ contribution shown in Figure 7.

The good agreement between theory and experiment in the line wings is evidence that large-angle scattering is correctly described by a hard sphere model. This result is consistent with large-angle scattering occurring for very close collisions where the alkali-rare gas potentials can be approximated by an infinite repulsive barrier. The failure of the theory near the narrow resonance for the heavier perturbers (Ne and Kr) is indicative of an interatomic potential that is other than hard sphere. Most likely there exist attractive wells in the Na⁺-Kr and Na⁺-Ne potentials that give rise to the additional scattering near the resonances.

The fact that the widths of the narrow resonance near $\Delta'/2\pi = 1.6$ GHz is generally larger than that predicted by the lineshape theory using empirically determined experimental values for all broadening parameters may be due to either (a) additional small angle velocity-changing collisions or (b) larger values of the broadening parameters caused by the faster selection of fast Na atoms. We should also note that our theory of the $3P_{3/2} \leftrightarrow 3P_{1/2}$ exchange is oversimplified and can lead to some additional errors.

The values for the hard sphere collision cross sections which we obtain exhibit the pressure dependence shown in Figure 15. The slow increase of the cross sections with increasing pressures is another indication that the theory is failing to properly account for the true collisional interaction. This variation implies that with increasing pressure the

amplitude of the resonance at $\Delta'/2\pi = 1.6$ GHz becomes increasingly overestimated by the theory leading to anomalously large values for the calculated collision cross sections. Whether this variation is due to our model for $3P_{3/2} \leftrightarrow 3P_{1/2}$ collisions, to effects of weak velocity-changing collisions, or to our failure to use speed-dependent broadening parameters is unknown at present. It would seem reasonable to consider the cross sections we obtained as upper bounds for the true cross sections.

The cross sections for collisions with neon and krypton are approximately 30 and 55 Å², respectively, and are similar to the values which can be deduced from ground state gas kinetic radii.¹⁷ The fact that the krypton cross section is larger is reasonable in light of its larger size and greater polarizability. The helium cross section of ~ 60 Å² on the other hand, does not fit this picture. The apparent helium cross section is the largest of the three measured cross sections within the estimated accuracy of our measurements of 30 to 40 percent despite the fact that the helium core is surely the smallest and the atom is the least polarizable. It should be noted, however, that we have arbitrarily chosen to fit the data at $\Delta' = 0$, where, because of the small velocity change produced by sodium-helium collisions, the contribution of the velocity changing signal (component b in Figure 2) is extremely small. Small errors in the calculation of component b will then result in substantial error in our result for the cross section. If instead, we fit the lowest pressure helium data at $\Delta'/2\pi = 1$ GHz, we find $\sigma = 35$ Å² in better relative agreement with our expectations. However, the optimum cross-section is still found to increase with pressure since the cross sections calculated at higher pressures are independent of where we fit the data.

V. CONCLUSION

We have examined the effects of velocity-changing collisions on the $35P_{3/2} \leftrightarrow 3P_{1/2}$ excitation spectra of sodium vapor. The observed lineshapes are reasonably well described by a theory in which collisions are characterized by either the phenomenological Keilson-Störmer kernel or a classical hard sphere kernel. For collisions between excited sodium atoms and heavy rare gas atoms, the hard-sphere kernel is superior to the Keilson-Störmer kernel. It gives a better description of the effects of large angle scattering although

neither kernel provides a fully adequate description over the entire profile. The two kernels give essentially the same lineshape for low active atom to perturber atom mass ratio. They also agree at high pressures independent of the mass ratio. Our data indicate that improved models are required to accurately describe sodium-rare gas collisions. By fitting our data we extract effective hard-sphere-collision cross sections for collisions between sodium $3P_{1/2}$ atoms and helium, neon, and krypton perturbers.

The research of one author (PKB) is supported by the U.S. Office of Naval Research.

APPENDIX

In this Appendix, collision kernels and rates for classical hard sphere scattering are derived. The collision kernel, $W(\vec{v}, \vec{v}')$, gives the probability density per unit time for a collision with the perturber bath to change the velocity of an "active atom" particle from \vec{v} to \vec{v}' is given by⁷

$$W(\vec{v}, \vec{v}') = N \left(\frac{m_e}{\mu} \right) \int d\vec{v}_p d\vec{v}_p' W_p(\vec{v}_p) v_p^{-1} \times \delta \left(\vec{v}_p + \frac{m_e}{m_p} \vec{v} - \frac{m_e}{\mu} \vec{v}' + \vec{v}_p' \right) \delta(v_p - v_p') f(\vec{v}_p, \vec{v}_p') \quad (A-1)$$

with

$$\vec{v}_p' = \vec{v} - \vec{v}_p; \quad \vec{v}_p'' = \vec{v}' - \vec{v}_p'$$

where m_e is the active atom mass, m_p the perturber mass, μ the reduced mass, \vec{v} (or \vec{v}') the active atom velocity, \vec{v}_p (or \vec{v}_p') the perturber velocity, $\int f(\vec{v}_p, \vec{v}_p') d\vec{v}_p d\vec{v}_p'$ is the differential scattering cross section, and $W_p(\vec{v}_p)$ the perturber velocity distribution assumed to be of the form

$$W_p(\vec{v}_p) = (\pi u_p^2)^{-3/2} \exp(-v_p^2/u_p^2); \quad (A-2a)$$

$$u_p^2 = 2kT/m_p; \quad (A-2b)$$

$$W(v_1, v_2) = \int d v_1 d v_2 W(v_1, v_2) W(v_1, v_2) \quad (A-12)$$

Substituting Equations (A-1) and (A-9) into (A-12) and carrying out the tedious but straightforward integrations, one may obtain

$$W(v_1, v_2) = \frac{1}{4} \pi r^2 N \frac{(1+\beta^2)}{\beta^2} \left\{ 1 - \Phi \left[\frac{1+\beta^2}{2\beta} r |S_1| + \frac{v_1^2}{u} \beta \frac{S_1}{|S_1|} \right] \right. \\ \left. + \exp \left[-r S_1 (S_1 + 2v_1/u) \right] \left[1 - \Phi \left[\frac{1-\beta^2}{2\beta} r |S_1| - \frac{v_1^2}{u} \beta \frac{S_1}{|S_1|} \right] \right] \right\} \quad (A-13)$$

where

$$\beta = u/u_p; \\ r = [\beta^2 + T_1 T_2] / (\beta^2 + 1).$$

If $T_1 = T_2$, then $r = 1$ and one arrives at Equation (12) of the text.

The rate, $\Gamma(v_2)$, defined by

$$\Gamma(v_2) = \int d v_1 W(v_1, v_2)$$

can be calculated as

$$\Gamma(v_2) = \pi r^2 N u_p \left\{ \left[\frac{v_2}{u_p} \right] \Phi \left[\frac{v_2}{u_p} \right] + \pi^{-1/2} \exp \left[- \left(\frac{v_2}{u_p} \right)^2 \right] \right. \\ \left. \times \left[1 + \pi^{1/2} \int_0^\infty \exp \left[- \frac{\beta^2 x^2}{(1+\beta^2)^2} \right] \cosh \left[\frac{2v_2 x}{u_p (1+\beta^2)^2} \right] \right. \right. \\ \left. \left. \times \left[1 - \Phi \left[\frac{x}{1+\beta^2} \right] \right] dx \right] \right\} \quad (A-14)$$

Equations (A-4), (A-8) and (A-13) have been derived previously by Kol'chenko.¹⁵ As noted in the text,¹¹ the use of one-dimensional kernels in the theory of saturation spectroscopy is not strictly valid when the collision rates are speed-dependent.

REFERENCES

- T. W. Hänsch and P. E. Toschek, *IEEE J. Quant. Elec.* **5**, 61 (1969); P. W. Smith and T. W. Hänsch, *Phys. Rev. Lett.* **26**, 740 (1971); R. Keil, A. Schabert and P. Toschek *Z. Phys.* **261**, 71 (1973); I. M. Beterov, Y. A. Matyugin and V. P. Chebotayev *Sov. Phys. JETP* **37**, 756 (1973).
- W. K. Bischel and C. K. Rhodes, *Phys. Rev.* **A14**, 176 (1976); C. Brechignac, *Phys. Rev. Lett.* **37**, 1311 (1976); R. Vetter, and P. R. Berman, *Phys. Rev. A* **17**, 1609 (1978); J. de Phys. T. Mossberg, A. Flusberg, R. Kachru and S. R. Hartman, *Phys. Rev. Lett.* **42**, 1665 (1979).
- C. N. Bagaev, E. V. Baklanov and V. P. Chebotayev, *JETP Lett.* **16**, 9 (1972); T. W. Meyer, C. K. Rhodes and H. A. Haus, *Phys. Rev.* **A12**, 1993 (1975); P. Cahuzac, O. Robaux and R. Vetter *J. Phys.* **B9**, 3165 (1975); A. T. Mattick, N. A. Kurmit, and A. Javan *Chem. Phys. Lett.* **38**, 176 (1976); P. Cahuzac, E. Marie, O. Robaux, R. Vetter, and P. R. Berman, *J. Phys.* **B 11**, 645 (1978).
- D. L. Huber, *Phys. Rev.* **178**, 93 (1969); A. Omont, E. W. Smith and J. Cooper, *Astrophys. J.* **175**, 185 (1972); J. L. Carlsten and A. Szöke, *Phys. Rev. Lett.* **36**, 667 (1976) and *J. Phys.* **B 9**, L231 (1976); J. L. Carlsten, A. Szöke and M. G. Raymer, *Phys. Rev. A* **15**, 1029 (1977); D. L. Rousseau, G. D. Patterson and P. F. Williams, *Phys. Rev. Lett.* **34**, 1306 (1975); R. D. Driver and J. L. Snider, *J. Phys.* **B 10**, S95 (1977).
- P. F. Liao, J. E. Bjorkholm and P. R. Berman, *Phys. Rev. A*, to be published.
- J. Keilson and K. E. Störer, *Q. Appl. Math.* **10**, 57 (1977).
- P. R. Berman, *Advances in Atomic and Mol. Phys.* **13**, 243 (1978).
- P. R. Berman, P. F. Liao and J. E. Bjorkholm, to be published.
- See, for example, J. E. Bjorkholm and P. F. Liao, *Phys. Rev.* **A14**, 751 (1976) and references therein.
- [10] See, for example, I. M. Beterov and V. P. Chebotayev, *Prog. Quant. Electr.* **3**, 1 (1974); R. Salomaa and S. Stenholm *J. Phys.* **B 8**, 1795 (1975); **9**, 1221 (1976).
- [11] The use of a one-dimensional kernel is not strictly valid in cases where the collision rates are speed-dependent. In order to reduce the equations to those of an effective one-dimensional problem in velocity space, one must be able to factor the density matrix into parts depending on the longitudinal and transverse velocity components. This factorization procedure fails for saturation spectroscopy with speed dependent rates; the pump laser field excites a nonthermal longitudinal velocity distribution which is transferred, in part, to the transverse velocity distribution via the speed dependence in the collision rate, (i.e., if one excites a "hot" longitudinal atom, part of this heat is transferred to the transverse velocity distribution via collisions). The errors introduced by using a one-dimensional kernel are probably not severe, considering the overall accuracy of the calculation.
- [12] M. Borenstein and W. E. Lamb, *Phys. Rev.* **45**, 1311 (1972).
- [13] J. L. LeGouët, *J. Phys.* **B 11**, 3001 (1978).
- [14] C. R. Borde, private communication.
- [15] A. P. Kol'chenko, S. G. Rautian and A. M. Shalagin, *Nuclear Phys. Inst. Semiconductor Physics Internal Report* (1972).
- [16] See Table I of Reference 5.
- [17] C. W. Allen, *Astrophysical Quantities*, 2 ed (Univ. of London, London, 1963), p. 45.

FIGURE CAPTIONS

4: Schematic diagram of the experimental setup. Although not shown, the light from laser I was chopped and the output of the photomultiplier (PMT) was processed with a lock-in amplifier.

5: Schematic representation of the observed lineshape in terms of three components. Component (a) is the "two-photon" line; components (b) and (c) are the collisionally-induced components, as discussed in the text.

6: The energy levels of the sodium atom relevant for our experiment. Not shown is the 1.77 GHz hyperfine splitting of the 3S ground state.

7: Probe laser excitation spectrum of the $3P_{3/2} - 4D_{3/2}$ transition with the pump laser tuned to the $3S_{1/2} - 3P_{1/2}$ transition. This signal is the result of fine-structure-state-changing collisions produced by 0.5 torr of neon perturber gas. The narrow linewidth demonstrates that fine-structure-state changes occur with negligible velocity change.

8: The steady-state axial-velocity distributions $n(v)$ for sodium atoms in the 3P states which have experienced exactly i collisions since being initially excited. The calculations were carried out for 2.5 torr of helium perturber gas, using both the hard-sphere and the Keilson-Störmer kernels. All curves have been normalized to the same height.

9: Same as Fig. 5, except the perturber gas is neon.

10: Same as Fig. 5, except the perturber gas is krypton.

11: Excitation spectrum of the $3S_{1/2} - 3P_{1/2} - 4D_{3/2}$ transition of atomic sodium in 5 torr of helium perturber gas. The pump laser was tuned such that $\Delta/2\pi = 1.6$ GHz. The solid (open) circles show the theoretical fit obtained using the hard-sphere (Keilson-Störmer) collision kernel.

Fig. 9: Same as Fig. 8, except for 2.5 torr of neon perturber gas.

Fig. 10: Excitation spectrum of the $3S_{1/2} - 3P_{1/2} - 4D_{3/2}$ transition of atomic sodium in a perturber gas of krypton. The pump laser was tuned such that $\Delta = 1.6$ GHz. The krypton pressure was 0.5 torr. The solid (open) circles show the theoretical fit obtained using the hard-sphere (Keilson-Störmer) collision kernel. The sharp resonances occurring for negative Δ' are due to the residual copropagating light, as discussed in the text.

Fig. 11: Same as Fig. 10, except krypton pressure was 2.5 torr.

Fig. 12: Same as Fig. 10, except the krypton pressure was 5 torr.

Fig. 13: The contribution of velocity-changing collisions to the excitation spectrum as a function of normalized velocity for 9.5 torr of helium perturber gas. The smooth curve is the difference between the experimental excitation spectrum and the theoretical contributions to the excitation spectrum from all sources except velocity-changing collisions. The solid circles give the contribution due to velocity-changing collisions as calculated using the hard-sphere kernel; the open circles give the same for the Keilson-Störmer kernel.

Fig. 14: Same as Fig. 13, except for 1 torr of krypton perturber gas. The hard sphere and Keilson-Störmer kernels now lead to significantly different profiles.

Fig. 15: Variation of the experimentally deduced cross sections for velocity-changing collisions between Na ($3P_{1/2}$) and He , Ne , and Kr perturbers as a function of perturber pressure.

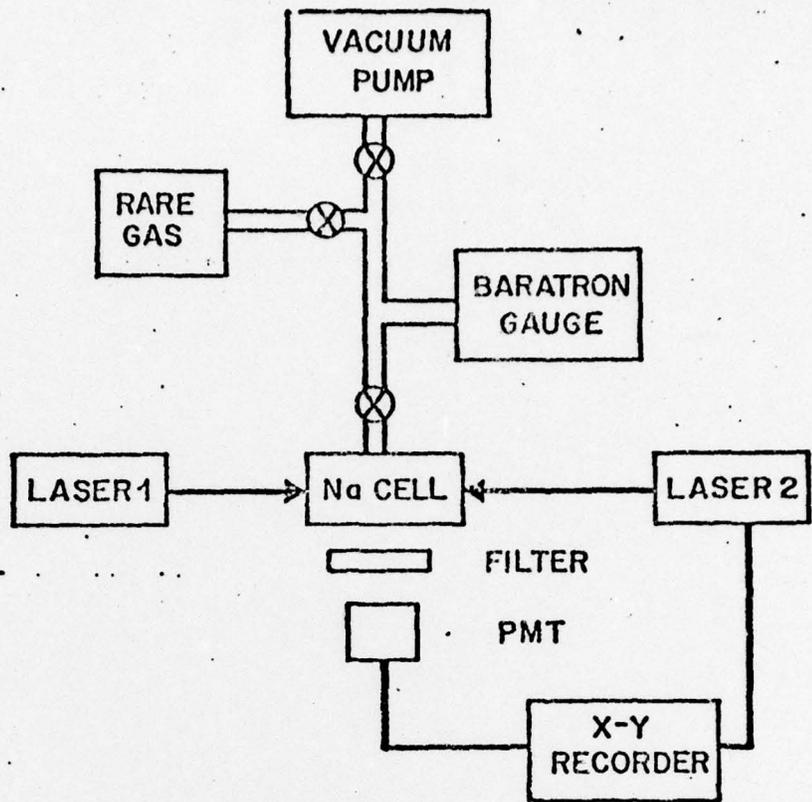


Fig 1

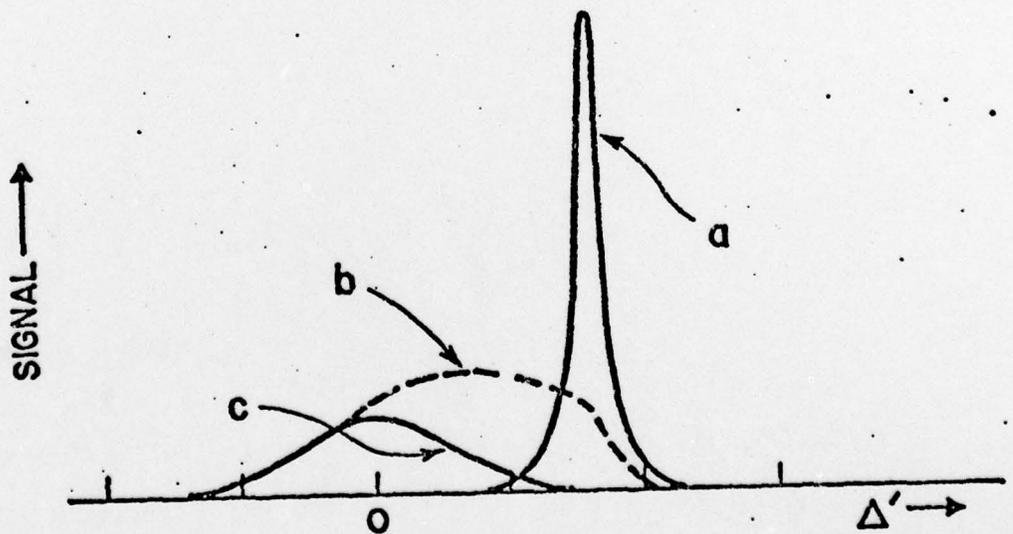


Fig 2

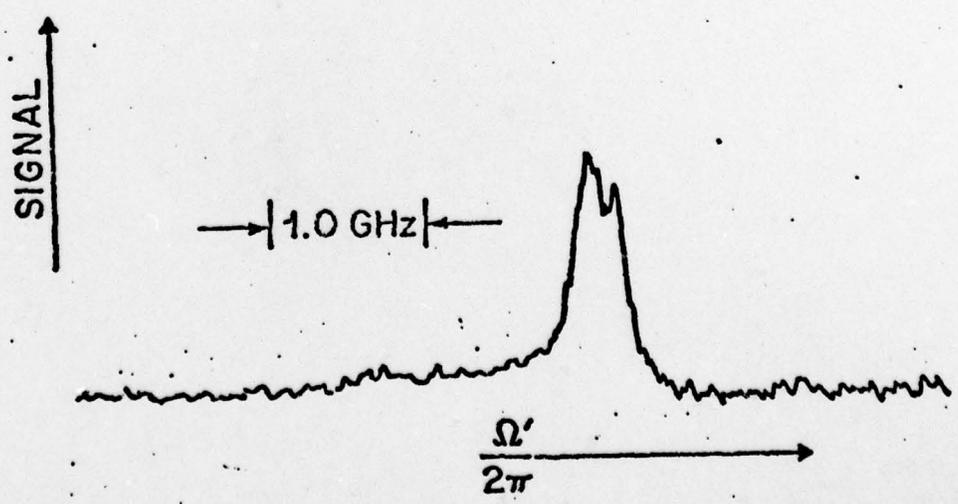
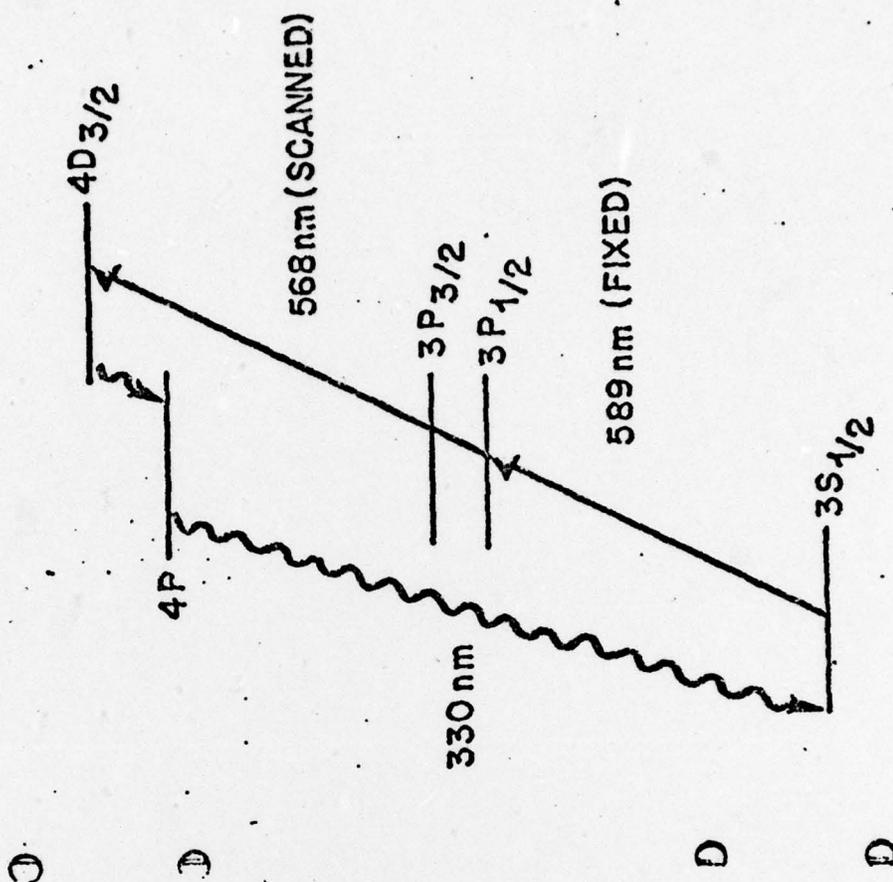
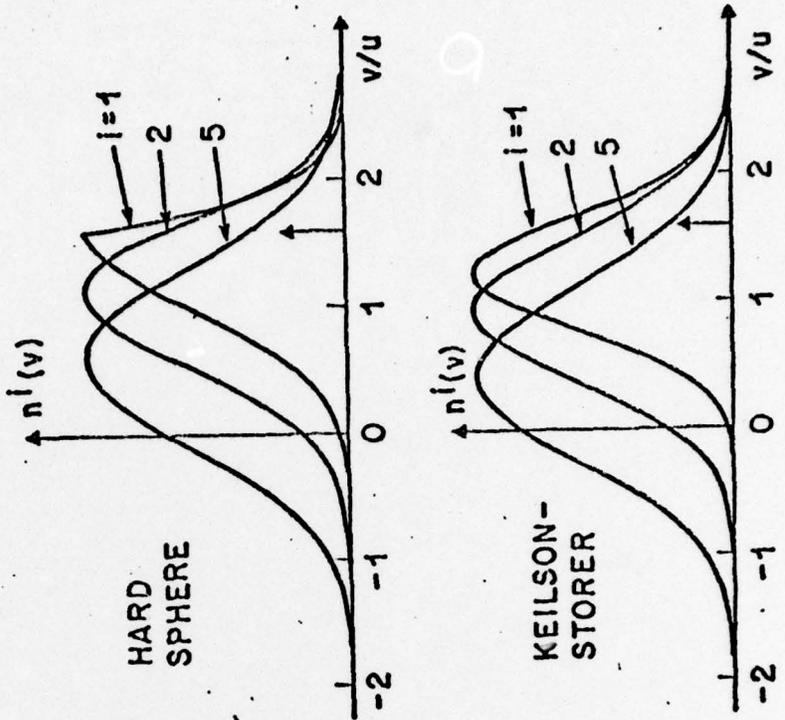


Fig 4

HELIUM - 2.5 TORR



NEON - 2.5 TORR

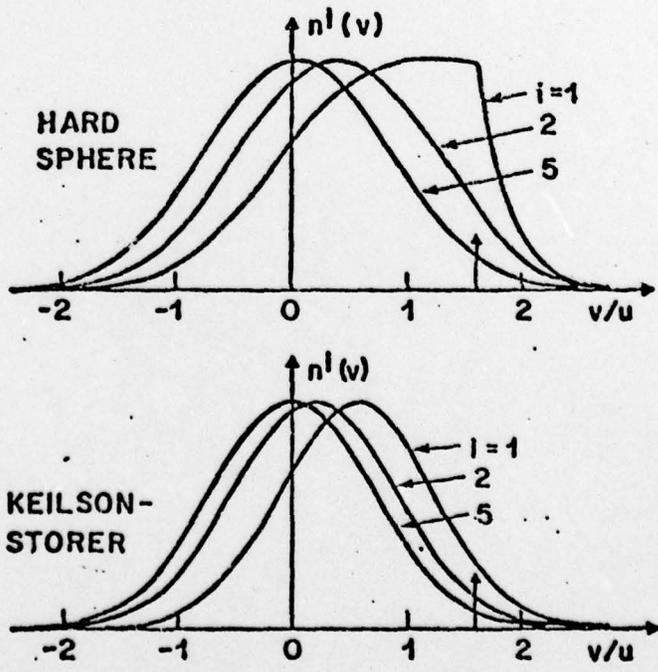
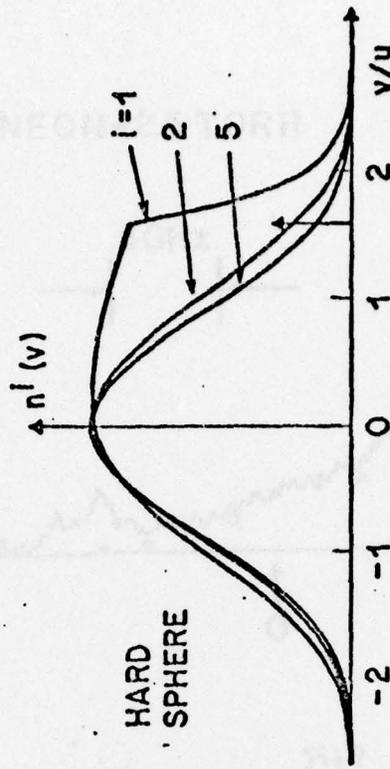
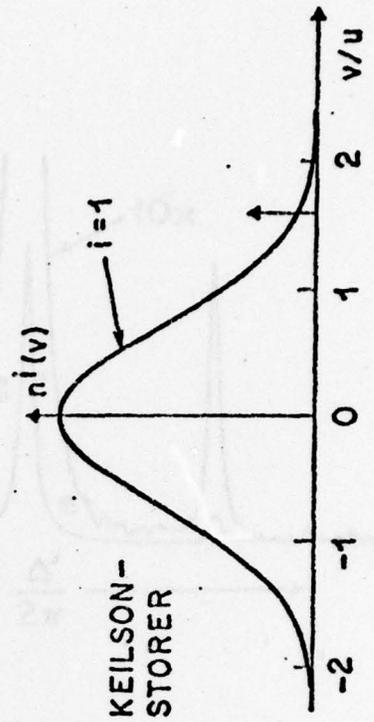


Fig 6

KRYPTON - 2.5 TORR



HARD
SPHERE



KEILSON-
STORER

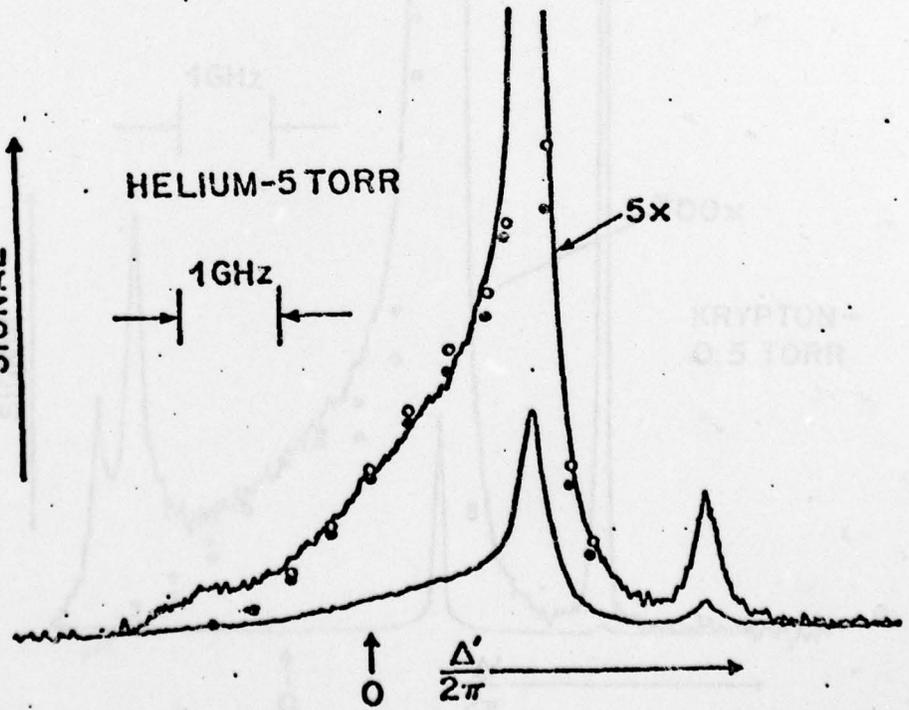
SIGNAL

HELIUM-5 TORR

1GHz

5x

KRYPTON
0.5 TORR



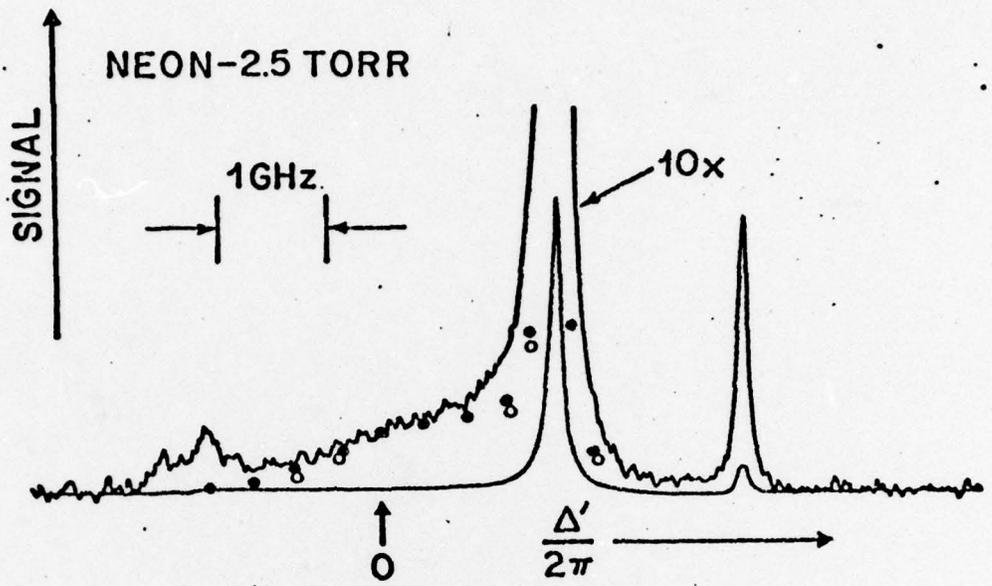


Fig 9

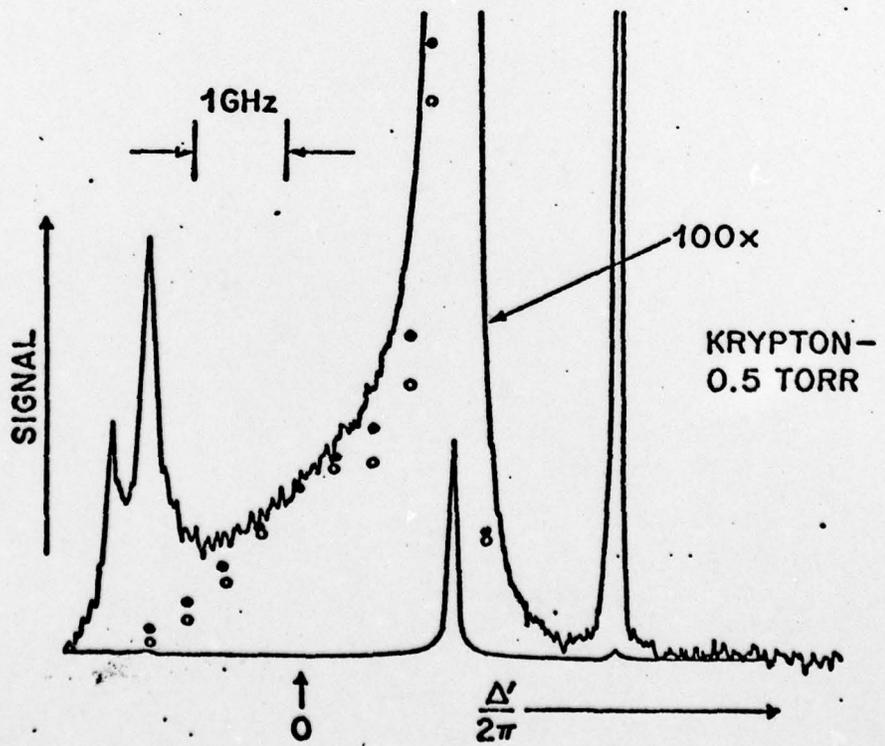


Fig 10

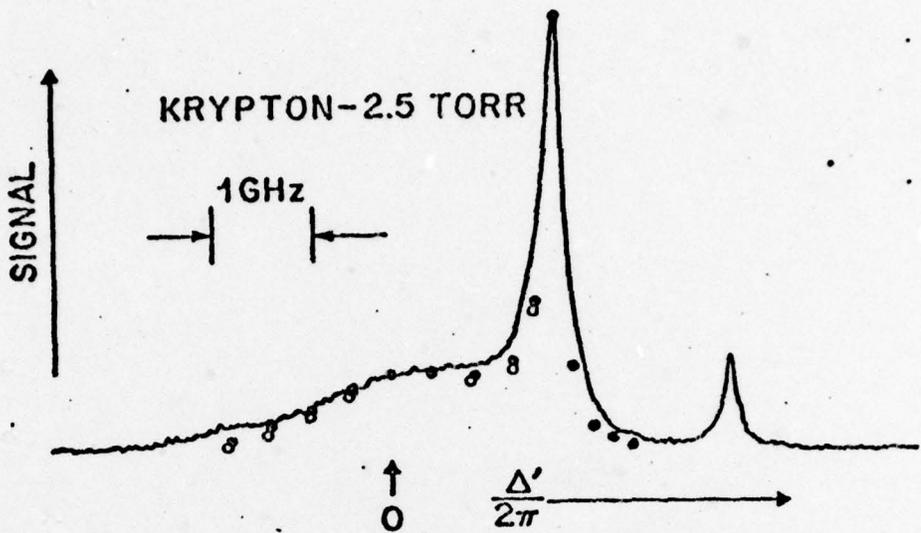


Fig 11

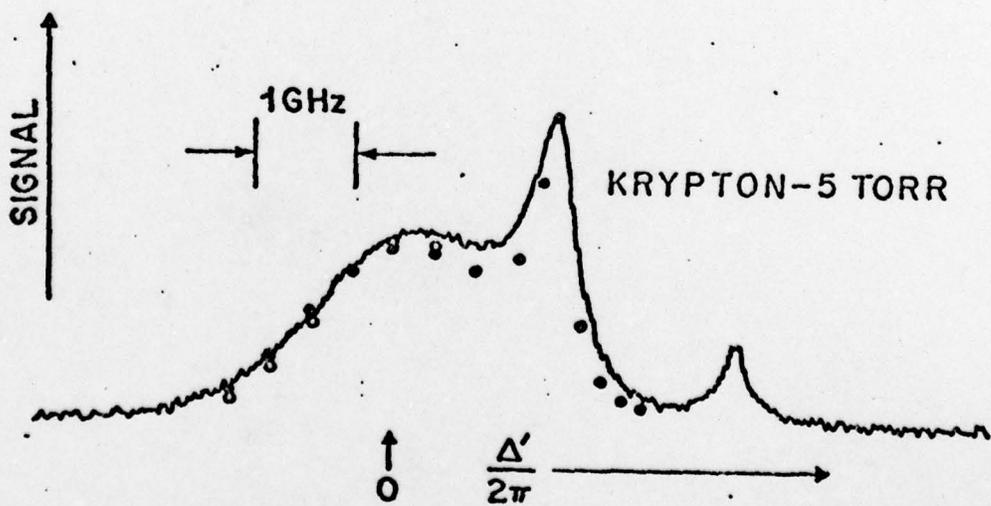


Fig 12

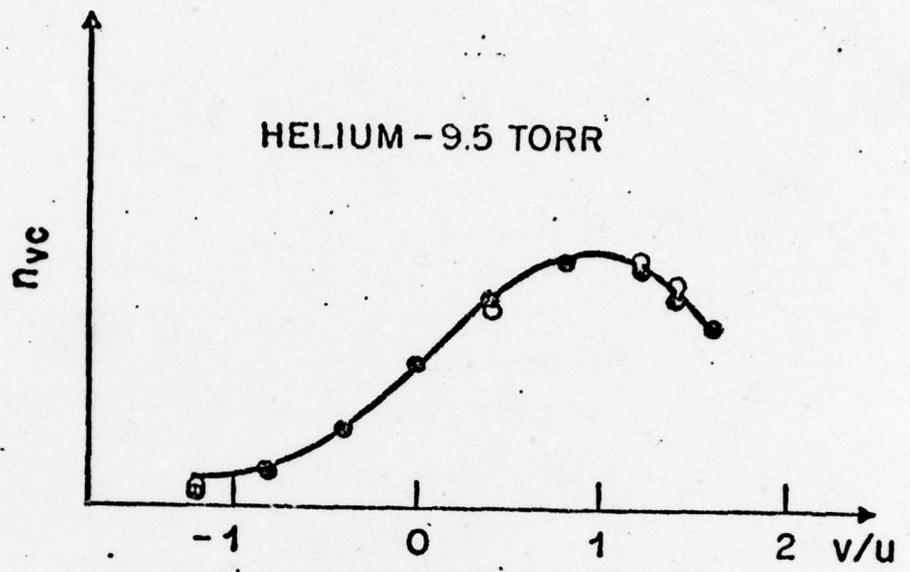


Fig 13

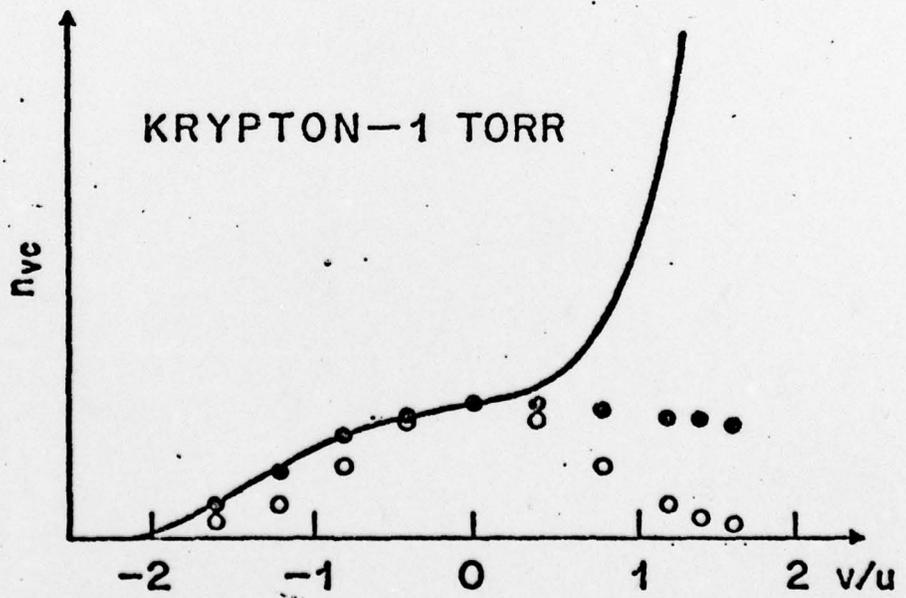


Fig 14

COLLISION CROSS-SECTION-Å²

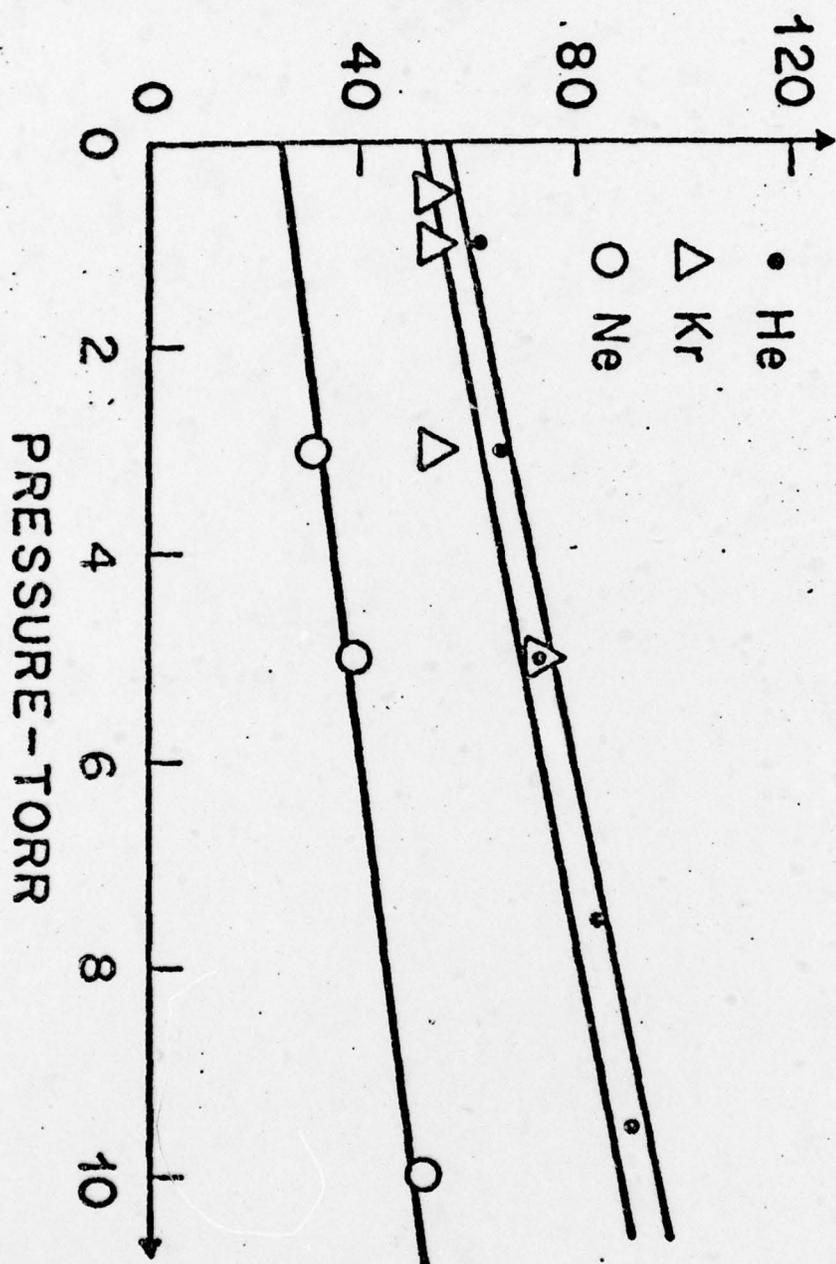


Fig. 15